Implementation of Sliding Mode Based-Direct Flux and Torque Control for Induction Motor Drive with Efficiency Optimization

Abdelkarim AMMAR[1 2], Tarek AMEID[3], Younes AZZOUG [2 3], Aissa KHELDOUN[1], Brahim METIDJI[1]
[1]Signals and Systems Laboratory (LSS), Institute of Electrical and Electronic Engineering, University of M'hamed BOUGARA of Boumerdes, Boumerdes, Algeria.
[2]Electrical Engineering Laboratory of Biskra (LGEB), Electrical Engineering Department, University of Mohamed KHIDER of Biskra, Algeria
[3] Faculty of Applied Science, Univ. Artois, EA 4025 LSEE F-62400, Béthune, France.
ammar.abdelkarim@yahoo.fr, tarek-gnr@hotmail.fr, azzougyounes@yahoo.fr, aissa.kheldoun@univ-boumerdes.dz, metidji77@yahoo.fr

Abstract

This paper presents an implementation of an efficient direct flux and torque control for induction motor drive. In control design, the modeling inaccuracy and various uncertainties cannot be avoided when classical methods are conducted. Therefore, it is recommended apply the nonlinear-robust control approaches to cover these drawbacks. The sliding mode approach is proposed to achieve a decoupled control and improve its robustness versus different disturbances. Furthermore, an optimal control algorithm is joined for losses minimization and efficiency maximization. This technique consists of the computation of optimum flux reference according to the load value and improves the efficiency for no load or light loads state, that makes is very suitable for variable load applications. The effectiveness of the control techniques is verified using an experimental test bench based on dSpace 1104 real-time interface.

Keyword: Induction motor, Direct torque control, Sliding mode control, Loss model control, dSpace 1104.

I. INTRODUCTION

Nowadays, the vector control methods became a viable control method in electric drives field. The direct torque control (DTC) offers a simpler structure, faster torque and higher robustness then the field-oriented control [1]. However, the basic DTC shows high flux/torque ripples and current harmonics due to the use of hysteresis comparators and look-up switching table for voltage vector selection. The replacement of the hysteresis comparators and switching table by linear controllers and PWM unit can fix the switching frequency and reduce ripples and switching losses [2]. However, this integration uses the stator-filed orientation principle that is employed in a non-stationary frame which may increase the complexity of control's algorithm by requesting coordinates transformation [3]. Besides, the use of linear controllers makes the control system so vulnerable to parameters variation that deteriorate control stability.

Recently, the use of advanced mathematical tools for automatic control application achieved an impressive development in the so-called nonlinear and robust control approaches. Many control methods have arisen in the past few decades such as the feedback linearization, backstepping and the sliding mode control [3], [4]. However, the application of the feedback linearization approach needs the exact knowledge of the mathematical model. In addition, its stability and robustness cannot be guaranteed while the presence of uncertainties [5]. The combination of the feedback linearization with the sliding mode control has been presented in [6]. This incorporation consists of applying the sliding mode control strategy on the resulting linearized system. The robustness and the discontinuous nature of variable structure control can overcome the drawbacks of feedback linearization technique and handle the sensitivity of the system due to parameters variation [7].

Despite the aforementioned advantages of the presented control strategies. The induction motor can perform higher performance by the maximum of efficiency. The control using constant reference of flux magnitude can be non-optimal for some operations, especially, concerning the power losses and the absorbed currents. In addition, the efficiency of the IM can be reduced when the reference flux is maintained to an initial value at light loads [8]. Therefore, the variable-flux reference is applied in many works. This operation can be able to optimize certain quantities without a significant degrading in dynamic performances. Among the main control algorithms which use an optimum flux level is the loss-model-based control (LMC) [9]. This method bases on the steady-state analysis and equivalent per-phase circuit to compute the optimal flux reference. The latter will be tuned according to the applied load increase the machine efficiency. This algorithm is faster and does not produce torque ripples [10]. However, its accuracy depends on the correct knowledge of machine parameters.

The main objective of this paper is the association of an efficiency maximization strategy based on losses minimization with a robust direct torque control scheme. The sliding mode control approach has been proposed to improve the robustness and to create an effective decoupled control. Furthermore, the LMC algorithm is used to computes the optimal flux reference according to the applied load value to minimize machines losses. The effectiveness of the global control technique is examined through an experimental implementation using dSpace 1104 board.

II. SLIDING MODE BASED SVM-DTC CONTROLLER DESIGN

A. Model presentation

The induction motor model can be rewritten as follows:

$$\dot{\mathbf{x}} = \mathbf{f}(x) + \mathbf{g}\mathbf{V_s} \tag{1}$$

$$\mathbf{x} = [i_{s\alpha} \quad i_{s\beta} \quad \psi_{s\alpha} \quad \psi_{s\beta}]^T \tag{2}$$

978-1-7281-2220-5/19/$31.00 ©2019 IEEE

$$\mathbf{V_s} = \begin{bmatrix} V_{s\alpha} & V_{s\beta} \end{bmatrix}^T \tag{3}$$

$$\mathbf{f}(x) = \begin{bmatrix} -\mu i_{s\alpha} - \omega_r i_{s\beta} + \dfrac{1}{\sigma L_s T_r}\psi_{s\alpha} + \dfrac{\omega_r}{\sigma L_s}\psi_{s\beta} \\ -\mu i_{s\beta} + \omega_r i_{s\alpha} + \dfrac{1}{\sigma L_s T_r}\psi_{s\beta} - \dfrac{\omega_r}{\sigma L_s}\psi_{s\alpha} \\ -R_s i_{s\alpha} \\ -R_s i_{s\beta} \end{bmatrix} \tag{4}$$

$$\mathbf{g} = \begin{bmatrix} \dfrac{1}{\sigma L_s} & 0 & 1 & 0 \\ 0 & \dfrac{1}{\sigma L_s} & 0 & 1 \end{bmatrix}^T \tag{5}$$

where:

$$\mu = -\frac{1}{\sigma}\left(\frac{R_r}{L_r} + \frac{R_s}{L_s}\right)$$

f(x) is the state variable function.[11]

$\mathbf{V}_s$ is the input voltage vector.

B. Sliding mode control design

The control design in this section is presented as a reformulation of SVM-DTC strategy using sliding mode approach. The flux and torque tracking errors represent the sliding surfaces as follows:

$$\begin{cases} S_1 = e_1 = T_e^{\,*} - T_e \\ S_2 = e_2 = \left|\psi_s^{\,*}\right|^2 - \left|\psi_s\right|^2 \end{cases} \tag{6}$$

To generate the sliding control law, the derivative of sliding surfaces can be written as follows:

$$\dot{S} = \begin{bmatrix} F_1 \\ F_2 \end{bmatrix} + \mathbf{C(x)} \begin{bmatrix} V_{s\alpha}^{\,*} \\ V_{s\beta}^{\,*} \end{bmatrix} \tag{7}$$

The switching function should be chosen in a manner to keep sliding mode behavior stable.

$$\dot{S} = -k_1 S - k_2 sign(S) \tag{8}$$

The sliding mode control law can be defined when the switching surface $S = 0$, by equalizing (7) and (8), we can obtain:

$$\mathbf{V_s} = \mathbf{C^{-1}}[-k_1 S - k_2 sign(S)] + \mathbf{C^{-1}F} \tag{9}$$

Then, the sliding mode control law can be written as:

$$\mathbf{V_s} = \begin{bmatrix} V_{s\alpha}^{\,*} \\ V_{s\beta}^{\,*} \end{bmatrix} = \begin{bmatrix} V_\alpha^{eq} \\ V_\alpha^{eq} \end{bmatrix} + \begin{bmatrix} V_\alpha^{d} \\ V_\beta^{d} \end{bmatrix} \tag{10}$$

The equivalent control can be expressed by:

$$\begin{bmatrix} V_\alpha^{eq} \\ V_\alpha^{eq} \end{bmatrix} = \mathbf{C(x)^{-1}} \begin{bmatrix} -F_1 \\ -F_2 \end{bmatrix} \tag{11}$$

The discrete control is defined as the auxiliary inputs:

$$\begin{bmatrix} V_\alpha^{d} \\ V_\beta^{d} \end{bmatrix} = \mathbf{C(x)^{-1}} \begin{bmatrix} -k_{11}S_1 - k_{12}sign(S_1) \\ -k_{21}S_2 - k_{22}sign(S_2) \end{bmatrix} \tag{12}$$

k_{11}, k_{12}, k_{21}, k_{22} are positive gains.

The global control law $\mathbf{V_s}$ is expressed as:

$$\begin{bmatrix} V_{s\alpha}^{\,*} \\ V_{s\beta}^{\,*} \end{bmatrix} = -C(x)^{-1} \begin{bmatrix} F_1 + k_{11}S_1 + k_{12}sign(S_1) \\ F_2 + k_{21}S_2 + k_{22}sign(S_2) \end{bmatrix} \tag{13}$$

For k_{11}, k_{12}, k_{21} and k_{22} positive, the stability can be ensured using Lyapunov function [12].

The smooth function s*igm(S)* is used instead the *sign(S)* in order to decrease the effect of chattering.

$$sigm(S) = \left(\frac{2}{1 + e^{\delta S}}\right) - 1 \tag{14}$$

δ is positive coefficient that adjusts the sigmoid function slope.

III. Application of Losses Minimization Strategy

A. Induction motor loss model in (d, q) reference frame

The equivalent circuit of the induction motor in shown in Fig.1. It is settled to the (*d, q)* coordinates frame which rotates synchronously with an electrical angular velocity ω_s. The copper losses are represented by the stator and rotor resistances R_s and R_r, whereas the iron losses are represented by the resistance R_c.

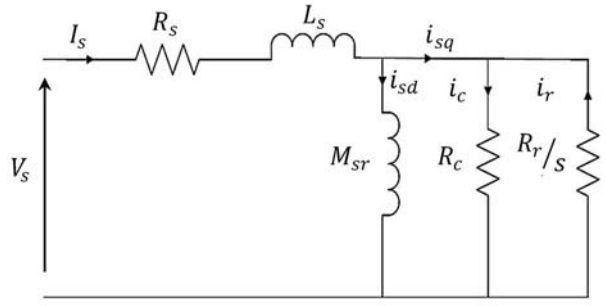

Fig.1 Induction motor equivalent circuit in (*d, q*) frame.

The machine losses can be computed in terms of direct and quadratic stator current components i_{sd} and i_{sq}, as follows:

$$P_{sc} = R_s i_s^2 = R_s (i_{sd}^2 + i_{sq}^2) \tag{15}$$

$$P_{rc} = R_r \left[\left(\frac{\psi_r}{L_r} - \frac{M_{sr}}{L_r} i_{sd} \right)^2 + \left(-\frac{M_{sr}}{L_r} \right)^2 \right] \tag{16}$$

P_{sc} and P_{rc} are stator and rotor copper losses respectively.

According to [13], the stator core losses in (*d, q*) reference frame are given by:

$$P_c = (\omega_s M_{sr})^2 \frac{1}{R_c} i_{sd}^2 \tag{17}$$

B. Loss minimization algorithm

The losses minimization algorithm bases on flux tuning to optimize the efficiency and minimize losses, especially at light load values [14]. In our work, the efficiency optimization consists of minimizing the stator and rotor copper losses in the steady state. The total copper losses are given as follows:

$$P_{c\_loss} = P_{sc} + P_{rc} \tag{18}$$

Based on rotor flux and electromagnetic torque expressions in (*d, q*) rotor field-oriented frame, the current components i_{sq} and i_{sd} can be written as:

$$i_{sd} = \frac{\psi_{rd}}{M_{sr}} \tag{19}$$

$$i_{sq} = \frac{T_e L_r}{p M_{sr} \psi_{rd}} \tag{20}$$

Then, the total losses expression can be written in terms of electromagnetic torque and rotor flux:

$$P_{c\_loss} = \frac{R_s}{M_{sr}^2}\psi_r^2 + \left[\frac{R_r}{p^2} + R_s\left(\frac{L_r}{pM_{sr}}\right)^2\right]\frac{T_e^2}{\psi_r^2} \tag{21}$$

By differentiating total copper losses expression with respect to the rotor flux to zero, the optimal flux can be founded [11].

$$\frac{\partial P_{c\_loss}}{\partial \psi_r} = 0 \tag{22}$$

Thus, the optimum reference value of the rotor flux can be computed as function of the reference torque and machine parameters by:

$$\psi_{r\_opt}^* = \lambda_{opt}\sqrt{T_e^*} \tag{23}$$

with

$$\lambda_{opt} = \left(\frac{\lambda_2}{\lambda_1}\right)^{1/4},\ \lambda_1 = \frac{R_s}{M_{sr}^2},\ \lambda_2 = \frac{R_r}{p^2} + R_s\left(\frac{L_r}{pM_{sr}}\right)^2$$

For the DTC control design, the stator flux reference value $\psi_{s\_opt}^*$ can be deduced by [15]:

$$\psi_{s\_opt}^* = \frac{L_s}{M_{sr}}\sqrt{\left(\psi_{r\_opt}^*\right)^2 + \left(\frac{\sigma L_r}{p}\right)^2\left(\frac{T_e^*}{\psi_{r\_opt}^*}\right)} \tag{24}$$

Fig.2 present block diagram of the optimized SMFL-DTC

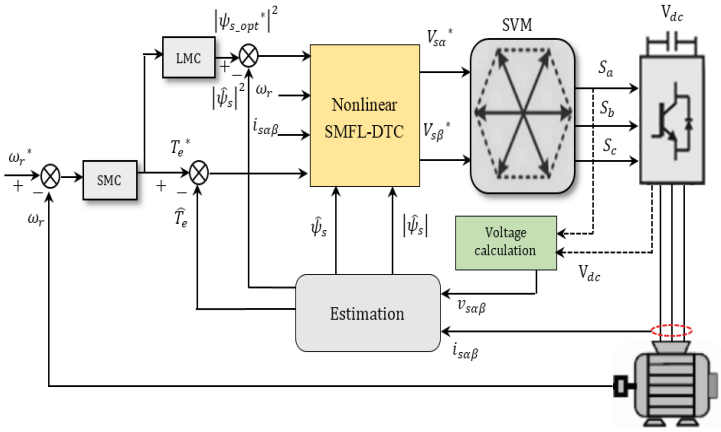

Fig.2 Block Diagram of SM-DTC with efficiency optimization strategy

IV. Experimental Results

The experimental test bench of the proposed control algorithm is presented in Fig.3. It contains: 1: A 1.1 kW asynchronous machine (The characteristics of the machine are given the appendix). 2: Semikron IGBT inverter. 3: an optical position and speed sensor 4: real-time interface dSpace 1104 5: Personnel computer with ControlDesk and MATLAB/Simulink software. 6: magnetic powder brake. 7 & 8: Hall effect current and voltage sensors. 9: digital scope.

Fig.3 Test bench description.

A. Starting up, steady state and load application

This section presents the performance analysis of the SMFL-DTC with constant and optimal flux references. The figures are specified ((a) for constant flux and (b) for optimal flux references).

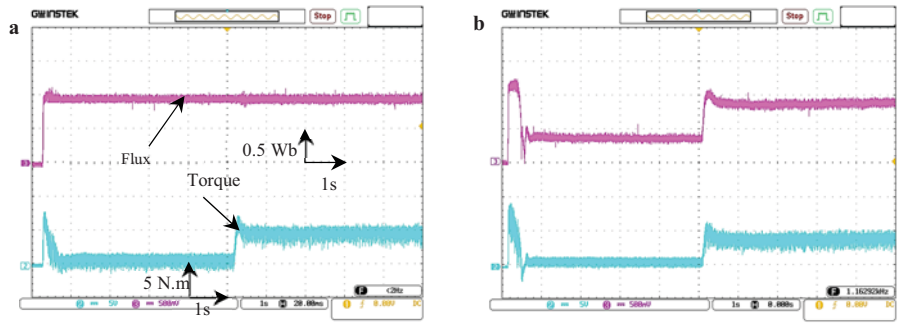

Fig.4 Stator flux magnitude [Wb] and electromagnetic torque [N.m].

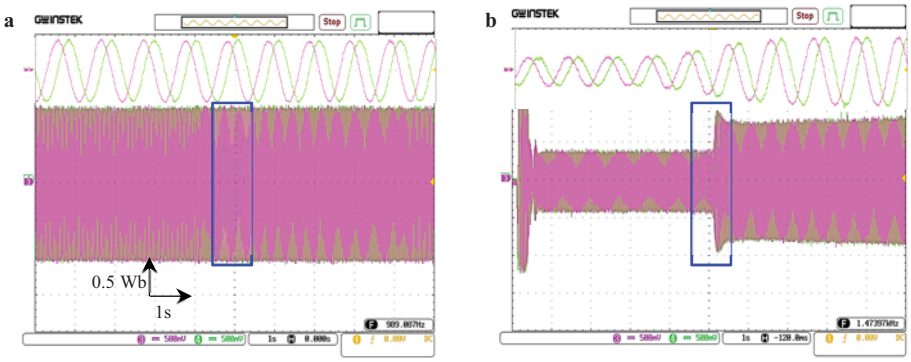

Fig.5 Stator flux components with zoom [Wb].

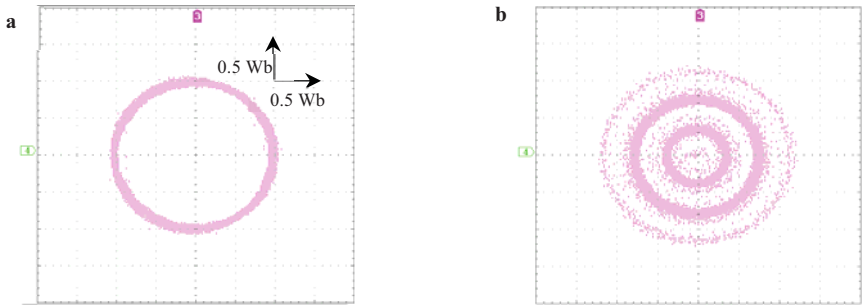

Fig.6 Stator flux trajectory [Wb].

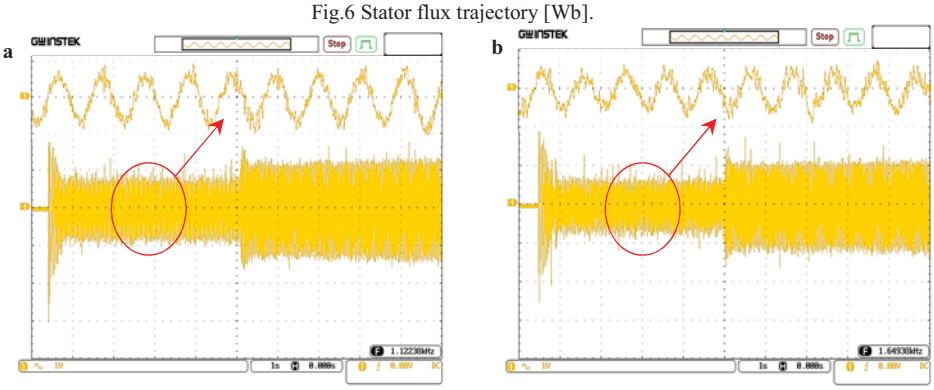

Fig.7 Stator phase current [A].

Fig.4 illustrates the flux magnitude (*0.5Wb=1div*) and the electromagnetic torque (*1div=5N.m*) during the starting up, steady state, then the load application of 4 N.m. The flux evolution is shown for the both cases of constant and optimal flux reference according to load value. It can be observed that the optimized technique has the reducer ripples level at no load and light load values. Figs.5-6 present the stator flux components and trajectory in both cases of constant and optimal flux reference in order to clarify more the evolution of flux due to load variation. Then, Fig.7 illustrates the stator phase current, it can be seen during no-load operation that the optimal control strategy provides a lower current amplitude than constant reference-based strategy. Hence, the copper losses can be minimized in this operation.

B. Application of different load values in steady state

This second phase presents efficiency computing and flux level estimation for both cases (i.e. constant and variable flux level) under different light load values, (*no-load, 0.5 N.m, 1 N.m, 1.5 N.m and 2 N.m*).

To understand more the instantaneous variation of flux level, Fig.8 presents flux evolution and torque response according to load application (0-*2 N.m*). Fig.9 illustrates the comparison of the calculated machine efficiency at *1200 rpm* of speed and *400 V* as input voltage. Then, Table.1 and Fig.10 summarized the efficiency analysis of the IM controlled by nonlinear SVM-DTC with energy optimization.

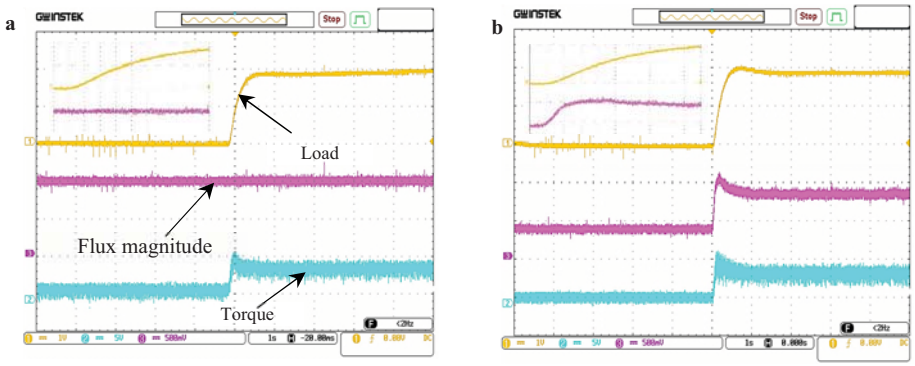

Fig.8 Flux and torque according to the applied load value (*0-2 N.m*).

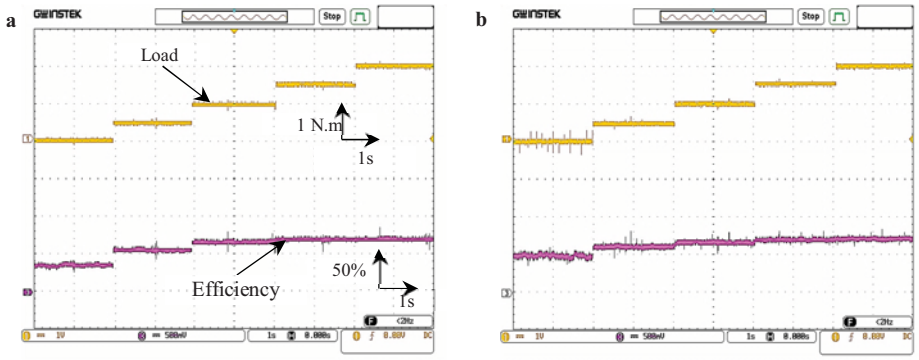

Fig.9 Load variation and Efficiency.

Table.1 motor efficiency analysis under different load values.

Load [N.m, %]	Constant flux		Optimal flux	
	Ψs [Wb]	η [%]	Ψs [Wb]	η [%]
0 (0%)	1	42	0.4	50.5
0.5 (7%)	1	60	0.55	64.9
1 (14%)	1	71.6	0.66	72.1
1.5 (21%)	1	75	0.75	75.5
2 (28%)	1	75.5	0.9	76.4

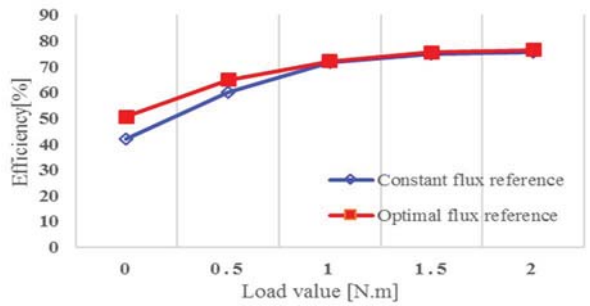

Fig.10 Curve of efficiency evolution according to different load values.

From Fig. 8-9 and the curve in Fig.10 and Table.1 we deduce the following summary: The flux level in case optimized by LMC strategy increases depending on the increase of load value to achieve the necessary torque. It can be seen that the effectiveness of the optimization strategy appears clearly at no or small loads, referring to the table (*0* to about *0.75 N.m*). Thereafter, this effectiveness decreases gradually with the increase in load value. We observed at *1 N.m* load that the difference between efficiencies has begun to diminish until their values have approached at *1.5 N.m load*. It can be concluded that the LMC strategy can be useful for low load applications. In addition, it has the ability to adjust the flux level for each rated load value.

V. Conclusion

The paper presents a design and experimental implementation of an optimized robust direct torque control based on losses minimization strategy (LMC) and sliding mode approach. The sliding mode control SM-DTC has been applied in order to solve the drawbacks of the classical strategy and realize decoupled flux and torque control to generate the reference voltages. Whilst, the losses model-

based algorithm has been presented in order to optimize IM energy by the online tuning of the flux reference.

The effectiveness and performance SM-DTC associated with losses minimization algorithm have been verified through the experimental implementation using dSpace real-time interface. It shows that LMC reduces losses and improves efficiency at zero and low load operations in the steady state. Therefore, the coupling of robust DTC algorithms with losses minimization can achieve high performances and efficiency for such applications that have variable loads.

APPENDIX

The parameters of the used three-phase Induction motor, in SI units are:

1.1kW, *50 Hz*, $p=2$, R_s=6.75Ω, R_r=6.21Ω, L_s=L_r=0.5192 H, M_{sr}= 0.4957 H, f_r=0.002 N·m·s, J=0.01240 kg·m².

The sampling frequency :10 kHz.
Inverter's switching frequency: 5 kHz.
DC link voltage: *Vdc= 537 V.*

REFERENCES

[1] F. Wang, Z. Zhang, X. Mei, J. Rodríguez, and R. Kennel, "Advanced control strategies of induction machine: Field oriented control, direct torque control and model predictive control," *Energies*, vol. 11, no. 1, 2018.

[2] Y.-S. Choi, H. H. Choi, and J.-W. Jung, "Feedback Linearization Direct Torque Control With Reduced Torque and Flux Ripples for IPMSM Drives," *IEEE Trans. Power Electron.*, vol. 31, no. 5, pp. 3728–3737, May 2016.

[3] A. Ammar, "Performance improvement of direct torque control for induction motor drive via fuzzy logic-feedback linearization," *COMPEL - Int. J. Comput. Math. Electr. Electron. Eng.*, p. COMPEL-04-2018-0183, Apr. 2019.

[4] K. Saad, K. Abdellah, H. Ahmed, and A. Iqbal, "Investigation on SVM-Backstepping sensorless control of five-phase open-end winding induction motor based on model reference adaptive system and parameter estimation," *Eng. Sci. Technol. an Int. J.*, no. xxxx, Mar. 2019.

[5] A. Accetta *et al.*, "Robust control for high performance induction motor drives based on partial state-feedback linearization," *IEEE Trans. Ind. Appl.*, vol. PP, no. 0, p. 1, 2018.

[6] C. Lascu, S. Jafarzadeh, M. S. Fadali, and F. Blaabjerg, "Direct Torque Control With Feedback Linearization for Induction Motor Drives," *IEEE Trans. Power Electron.*, vol. 32, no. 3, pp. 2072–2080, Mar. 2017.

[7] A. Devanshu, M. Singh, and N. Kumar, "Sliding Mode Control of Induction Motor Drive Based on Feedback Linearization," *IETE J. Res.*, vol. 2063, pp. 1–14, 2018.

[8] M. Hajian, G. R. Arab Markadeh, J. Soltani, and S. Hoseinnia, "Energy optimized sliding-mode control of sensorless induction motor drives," *Energy Convers. Manag.*, vol. 50, no. 9, pp. 2296–2306, Sep. 2009.

[9] F. Abrahamsen *et al.*, "On the Energy Optimized Control of Standard and High-Efficiency Induction Motors in CT and HVAC Applications," vol. 34, no. 4, pp. 822–831, 1998.

[10] M. N. Uddin, S. Member, and S. W. Nam, "New Online Loss-Minimization-Based Control of an Induction Motor Drive," vol. 23, no. 2, pp. 926–933, 2008.

[11] J.-F. Stumper, A. Dotlinger, and R. Kennel, "Loss Minimization of Induction Machines in Dynamic Operation," *IEEE Trans. Energy Convers.*, vol. 28, no. 3, pp. 726–735, Sep. 2013.

[12] A. Ammar, A. Bourek, and A. Benakcha, "Robust SVM-direct torque control of induction motor based on sliding mode controller and sliding mode observer," *Front. Energy*, Jan. 2017.

[13] S. Lim and K. Nam, "Loss-minimising control scheme for induction motors," *IEE Proc. - Electr. Power Appl.*, vol. 151, no. 4, p. 385, 2004.

[14] A. Baba, E. Mendes, and A. Razek, "Losses minimisation of a field-oriented controlled induction machine by flux optimisation accounting for magnetic saturation," in *1997 IEEE International Electric Machines and Drives Conference Record*, 1997, no. 1, p. MD1/2.1-MD1/2.3.

[15] F. Tazerart, Z. Mokrani, D. Rekioua, and T. Rekioua, "Direct torque control implementation with losses minimization of induction motor for electric vehicle applications with high operating life of the battery," *Int. J. Hydrogen Energy*, vol. 40, no. 39, pp. 13827–13838, Oct. 2015.